Comparative NMR study of hybridization effect and structural stability in $D0_{22}$-type $NbAl_3$ and $NbGa_3$

C. S. Lue,* T. H. Su, B. X. Xie, and C. Cheng
Department of Physics, National Cheng Kung University, Tainan 70101, Taiwan
(Received 28 June 2006; published 11 September 2006)

With the aim of providing experimental information for the correlation between *p-d* hybridization and phase stability in the $D0_{22}$ structure, we performed a comparative investigation on $NbAl_3$ and $NbGa_3$ using ^{93}Nb NMR spectroscopy. The quadrupole splittings, Knight shifts, and spin-lattice relaxation times (T_1's) for each individual compound have been identified. The larger quadrupole interaction and higher anisotropic Knight shift have been observed in $NbAl_3$, indicative of the stronger hybridization effect for this material, as compared with its isostructural compound $NbGa_3$. Results of experimental T_1 together with theoretical band structure calculations provide a measure of *d*-character Fermi-level density of states $N_d(E_F)$ and an indication of orbital weights. In addition, we found evidence that $N_d(E_F)$ correlates with the structural stability of the studied materials. Our NMR measurements confirm that $NbAl_3$ is more stable than $NbGa_3$ with respect to the $D0_{22}$ structure, attributed to the stronger *p-d* hybridization in the former material.

DOI: 10.1103/PhysRevB.74.094101 PACS number(s): 76.60.−k, 71.20.Be

I. INTRODUCTION

The $D0_{22}$ crystal structure (body-centered tetragonal) for the MX_3 compounds is a superstructure which consists of a stacking of two $L1_2$ cubes with the same antiphase shifts every two cubes, as shown in Fig. 1. There are two nonequivalent *X* sites and one single *M* site within this phase. Studies on the $D0_{22}$-type intermetallics, especially the transition metal-based trialuminides (MAl_3) such as $TiAl_3$, $NbAl_3$, and $TaAl_3$, are both of scientific and technological interests for potential aerospace applications. However, their poor ductility and toughness at low temperatures still need to be improved. Hence, the possible mechanisms driving the atomic ordering have attracted a large number of investigations, focused on electronic properties in the related alloys, to elucidate their structural phase stability.[1–11]

Theoretically electronic structure calculations have been performed to understand the stable phase in several $D0_{22}$-type transition metal trialuminides.[12–15] The calculated total density of states (DOS) exhibited a deep valley in the vicinity of the Fermi level, attributed to the hybridization between Al-*p* and *M-d* playing an important role for the DOS reduction. Nevertheless, there has been little experimental work associated with these scenarios, essential to interpret their hybridization effects and structural stability.

To gain experimental insight into the correlation between *p-d* hybridization and structural stability in $D0_{22}$, we thus select to compare $NbAl_3$ with $NbGa_3$, as both materials are isostructural. With the study of interactions between Nb *d* electrons and Al/Ga *p* electrons, the results can be utilized to examine the effect of *p* electrons on the hybridization of $D0_{22}$. In this paper, we will present ^{93}Nb NMR measurements including the Knight shifts, quadrupole transitions, as well as spin-lattice relaxation times in $NbAl_3$ and $NbGa_3$ as related to their electronic characteristics. In a parallel study, *ab initio* calculations were also performed to obtain the electronic DOS for comparison.

II. EXPERIMENT AND DISCUSSION

Polycrystalline samples were prepared from 99.9% Nb, 99.99% Al, and 99.999% Ga by mixing appropriate amounts of elemental metals, pressing the mixtures into small pellets, and melting them in an Ar arc furnace. Each material was melted several times, and the weight loss during melting is less than 0.5%. To promote homogeneity, both compounds were annealed in a vacuum-sealed quartz tube at 900 °C for 7 days, and followed by furnace cooling. The resulting ingots, which tend to be brittle, were grounded to powder. A room-temperature x-ray diffraction was taken with Cu K_α radiation on powder samples. Strong reflections in both alloys could be indexed according to the expected $D0_{22}$ structure. Several weak peaks remain unidentified which had little effect on the NMR measurements. A more detailed analysis of the x-ray data, in which the $D0_{22}$ structure was refined with the Rietveld method. We thus obtained the lattice constants $a=3.80$ Å and $c=8.75$ Å for $NbAl_3$, and $a=3.75$ Å and $c=8.71$ Å for $NbGa_3$. These values were found to be close to those reported in the literature.[16]

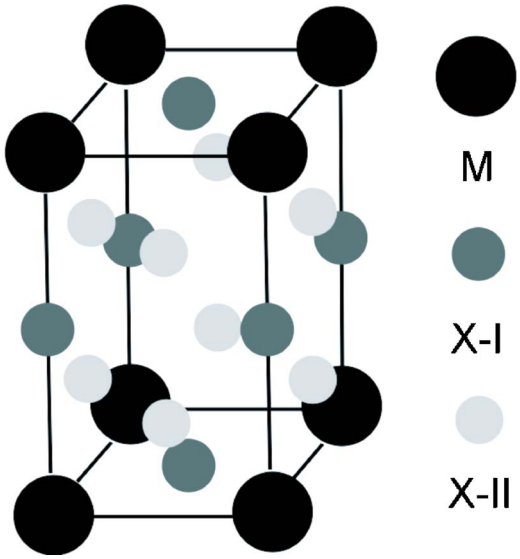

FIG. 1. (Color online) Crystal structure for the $D0_{22}$-type MX_3.

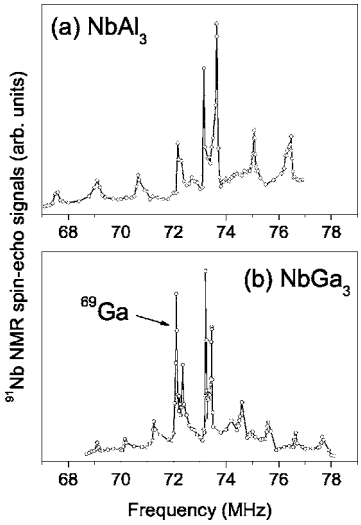

FIG. 2. Resolved satellite line shapes for the Nb site in $NbAl_3$ and $NbGa_3$.

NMR measurements were performed using a Varian 300 spectrometer, with a constant field of 7.05 T. A home-built probe was employed for both room-temperature and low-temperature experiments.[17–19] Since the studied materials are metals, powder samples were used to avoid the skin depth problem of the rf transmission power. Each specimen was set in a plastic vial that showed no observable ^{93}Nb NMR signal. The Knight shifts here were referred to as the ^{93}Nb resonance frequency of aqueous $KNbCl_6$.

A. Quadrupole interactions and Knight shifts

Since the ^{93}Nb NMR resonance is extremely quadrupolar broadened, the wide-line satellite spectra were mapped out by integrating spin-echo signals of various excitations. For each studied material, there is a single Nb site which is axially symmetric, leading to a symmetric one-site NMR spectrum. Due to electric quadrupole coupling, the ^{93}Nb NMR spectrum $\left(I=\frac{9}{2}\right)$ consists of nine transition lines, as demonstrated in Fig. 2. For powdered samples, as in our experiment, these lines appear as typical powder patterns, with distinctive edge structures corresponding to the quadrupole parameters. Since the first order quadrupole shift is the main effect shaping the satellite line, the quadrupole frequency, ν_Q, was determined directly from these lines. Results were tabulated in Table I. For $NbAl_3$, we only showed partial ^{93}Nb satellite lines because the high frequency side is strongly mixed with the ^{27}Al NMR signals.

TABLE I. Quadrupole frequency (MHz), isotropic and axial Knight shifts (%), and d and orbital electrons $(1/T_1T)$ $(s^{-1}\ K^{-1})$ for each studied alloy.

Alloy	ν_Q	K_{iso}	K_{ax}	$(1/T_1T)_d$	$(1/T_1T)_{orb}$
$NbAl_3$	2.90	−0.24	−0.025	0.126	0.027
$NbGa_3$	2.17	−0.38	0.009	0.184	0.041

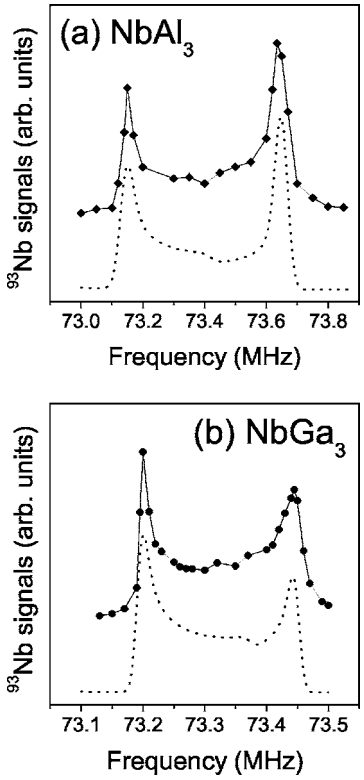

FIG. 3. ^{93}Nb central transition NMR spectra for $NbAl_3$ and $NbGa_3$ measured at room temperature. The dotted curves are simulated according to Eq. (1).

From ν_Q, we can determine the electric field gradient (EFG) for each material. Here $\nu_Q=3eQV_{zz}/2I(2I-1)h$ is defined by the nuclear quadrupole moment Q and the largest principal axis component of the EFG tensor V_{zz}. This effect arises from the noncubic arrangement of the charged lattice ions and the nonuniform charge density of the conduction electrons due to orbital motion. Attempts to reproduce the observed EFG's with a simple point-charge model yield unreasonable charge transfers. In fact, the electronegativity difference between Nb and Al/Ga atoms is low and hence the ionicity does not play a significant role on bonding nature of the studied compounds. On this basis, the valence charges would be the major source for the observed EFG's. The observed large EFG is attributed to the concentration of bonding charges in the *ab* planes. This interpretation is consistent with the previous ^{27}Al NMR studies of the $D0_{22}$ trialuminides, which pointed to larger directional bonding between transition metal and Al site-I.[7] Thus, due to the covalent interaction between Al/Ga-p and Nb-d electrons, both $NbAl_3$ and $NbGa_3$ should be considered as poor metals with covalent characters.

Central transition $\left(m=\frac{1}{2}\leftrightarrow-\frac{1}{2}\right)$ line shapes for $NbAl_3$ and $NbGa_3$ were given in Fig. 3. Each spectrum splits into two peaks because of the simultaneous presence of anisotropic Knight shift and second-order quadrupole interactions. In the $D0_{22}$ structure, the ^{93}Nb quadrupole shift and the angle-dependent Knight shift are axial. Hence the frequency shift for the central transition, $\Delta\nu$, to the second order quadrupole interaction and Knight shift can be written as[20]

TABLE II. Calculated Nb partial Fermi level *s*, *p*, and *d* DOS (states/eV atom) for each individual compound.

Alloy	*s*	*p*	*d*
$NbAl_3$	0.00016	0.01	0.307
$NbGa_3$	0.00028	0.01	0.370

$$\frac{\Delta\nu}{\nu_o} = \frac{K_{ax}}{1+K_{iso}}(3\cos^2\theta - 1) + \frac{\nu_Q^2}{16\nu_o^2}\left(I(I+1) - \frac{3}{4}\right)(1-\cos^2\theta) \times (1 - 9\cos^2\theta), \quad (1)$$

where ν_o is the Larmor frequency, K_{iso} is the isotropic Knight shift, K_{ax} is the axial Knight shift, and θ is the angle between the crystal symmetry axis and the external magnetic field. For a polycrystalline sample, shape function fitting for the case of combined quadrupole and axial shift interactions was presented first by Jones *et al.*[21] By substituting the determined ν_Q and tuning K_{ax}, each synthetic profile which matches well with the experimental ^{93}Nb NMR spectrum, was drawn as a dashed line in Fig. 3. The best-simulated results yielded the corresponding room-temperature values for K_{iso} and K_{ax}, as summarized in Table I.

The isotropic Knight shift here can be expressed as $K_{iso} = K_{orb} + K_d$. Here K_{orb} represents the orbital Knight shift, and K_d the *d*-spin shift which is negative due to the negative hyperfine field associated with the core-polarization via *d* electrons.[22–24] For both materials, the determined K_{iso} values are negative, indicative of a significant contribution from *d* states on the frequency shift. While the *s*-contact Knight shift (K_s) is usually comparable with K_d in *d*-electron based materials, we omitted this term because of the extremely low Fermi-level *s*-DOS for the present compounds. Indeed, calculated partial Fermi-level DOS (see Table II) confirms that Nb Fermi-level *d*-DOS are considerable larger than *s*-DOS for both $NbAl_3$ and $NbGa_3$ within the $D0_{22}$ structure. With this respect, an observation of the smaller absolute value of K_{iso} in $NbAl_3$ seems to suggest that this material contains a lower Nb Fermi-level *d*-DOS as compared with $NbGa_3$.

In an environment of axial symmetry, the anisotropic Knight shift $K_{an} = \frac{1}{2}K_{ax} = \frac{3}{2}(K_c - K_{ab})$, with K_c and K_{ab} corresponding to the Knight shifts in the *c* direction and *ab* plane, respectively. From this investigation, we found a larger absolute value of K_{an} in $NbAl_3$, indicating that the directional bonding is stronger in the basal plane of this compound, being consistent with the EFG results. Thus the anisotropic Knight shift together with the EFG analyses confirm the stronger *p*-*d* hybridization for $NbAl_3$, as compared to its isostructural compound $NbGa_3$.

B. Spin-lattice relaxation rates

The spin-lattice relaxation time (T_1) measurements were carried out using the inversion recovery method. We recorded the signal strength by integrating the recovered spin-echo signal. In these experiments, the relaxation process involves the adjacent pairs of spin levels, and the corresponding spin-lattice relaxation is a multiexponential expression.[25] For the central transition with $I = \frac{9}{2}$, the recovery of the nuclear magnetization follows

$$\frac{M(t) - M(\infty)}{M(\infty)} = -2\alpha(0.152e^{-t/T_1} + 0.14e^{-6t/T_1} + 0.153e^{-15t/T_1} + 0.192e^{-28t/T_1} + 0.363e^{-45t/T_1}), \quad (2)$$

derived from the initial conditions used in our experiments. Here $M(t)$ is the magnetization at the recovery time t and $M(\infty)$ is the magnetization after long time recovery. The parameter α is a fractional value derived from the initial conditions used in our experiments. Our T_1 values were thus obtained by fitting to this multiexponential recovery curve. To provide accurate values, each T_1 has been measured several times and the averaged T_1 for each individual material is enumerated in Table I. While nonconduction mechanisms may contribute to the relaxation, they were excluded by the Korringa relation (constant T_1T).[26] T_1 measurements performed at various temperatures yield Korringa behavior, indicating a conduction-electron mechanism for the observed relaxation.

As in the case of K_{iso}, two relaxation mechanisms dominate the ^{93}Nb T_1: $(1/T_1) = (1/T_1)_{orb} + (1/T_1)_d$. The first term is the orbital relaxation rate, while the second is due to *d*-spin interactions. For D_{4h} symmetry, which is the Nb-site symmetry in the $D0_{22}$ structure, a general expression for $(1/T_1)_d$ is[27]

$$\left(\frac{1}{T_1}\right)_d = 2hk_BT(\gamma_n H_{hf}^d)^2(n_{A_{1g}}^2 + n_{B_{1g}}^2 + n_{B_{2g}}^2 + 2n_{E_g}^2), \quad (3)$$

where h, k_B, and T are the Planck constant, Boltzmann constant, and absolute temperature, respectively. γ_n is the Nb nuclear gyromagnetic ratio and H_{hf}^d is the hyperfine field per electron of the Nb-*d* electrons. The terms $n_{A_{1g}}$, $n_{B_{1g}}$, $n_{B_{2g}}$, and n_{E_g} are Fermi-level DOS corresponding to the irreducible representations of the D_{4h} group, defined so that the total Fermi-level *d*-DOS $N_d(E_F) = n_{A_{1g}} + n_{B_{1g}} + n_{B_{2g}} + 2n_{E_g}$. Of these four representations, E_g contains two *d* orbitals, while the others contain one orbital each. However, the E_g orbitals in $D0_{22}$ play a minimal role on $(1/T_1)_d$, as concluded from an analysis of ^{51}V NMR T_1 on the isostructural compound VAl_3.[28] Therefore, with little orbital mixing, which is the case for Nb in $D0_{22}$, the square bracket in Eq. (3) becomes simply $N_d^2(E_F)$.

For $NbAl_3$ and $NbGa_3$, the values of $N_d(E_F) = 0.307$ and 0.370 states/eV atom have been determined from the first-principle electronic structure calculations, as presented later. Taking $H_{hf}^d \sim -2.1 \times 10^5$gauss in Nb metal,[22] the $(1/TT_1)_d$ values of 0.126 and 0.184 $s^{-1}K^{-1}$ for $NbAl_3$ and $NbGa_3$ were obtained. The orbital part can be thus isolated using $(1/TT_1)_{orb} = (1/TT_1) - (1/TT_1)_d$, giving the results listed in Table I. As indicated from Table I, the deduced values of $(1/TT_1)_{orb}$ were found to be much smaller than that of $(1/TT_1)_d$. Such a result is consistent with at most a few percent mixture of doubly degenerate E_g, using the parameters described above. We thus conclude that the dominant orbital at the Fermi level has a degeneracy close to unity for the $D0_{22}$ structure.

C. Electronic structure calculations

Theoretical studies with *ab initio* calculations were employed to obtain the total density of states for both $NbAl_3$ and $NbGa_3$ as well as the orbital projected partial density of states of Nb atoms in the systems. Total energy of the systems were determined in the framework of density functional theory.[29] The proposed generalized gradient approximation (GGA) by Perdew and Wang[30] was used for the nonlocal correction to a purely local treatment of the exchange-correlation potential and energy. The single-particle Kohn-Sham equations[31] were solved using the plane-wave-based Vienna *ab initio* simulation program (VASP) developed at the Institut für Material Physik of the Universität Wien.[32] The interactions between the ions and valence electrons are described by the projector augmented-wave (PAW) method[33] in the implementation of Kresse and Joubert.[34] The numbers of treated valence electrons are 11, 3, and 13 for Nb, Al, and Ga atoms, respectively. That is, the $3p$ ($3d$) electrons were also treated as valence electrons for Nb (Ga) atoms. The energy cutoffs for the plane-wave basis is 385 eV in all calculations. The Monkhorst-Pack[35] method of sampling k points is used for the Brillouin-zone integration.

The calculated lattice constants for the $D0_{22}$ structure of $NbAl_3$ ($NbGa_3$) are $a=3.847$ (3.828) Å and $c=8.632$ (8.817) Å. These results compare well with the experimental values for $NbAl_3$ and $NbGa_3$.[16] The Monkhorst-Pack parameters (13 13 5) were used for the unit cells which consist of two Nb atoms six Al (or 6 Ga) atoms in structural optimization as well as the calculations of density of states.

The calculated total density of states as well as the orbital projected partial density of states for Nb atoms for both systems are presented in Fig. 4. The partial Fermi-level DOSs for the s, p, and d electrons of niobium atoms are tabulated in Table II. The density of states in the deep levels are not shown in the figure which include the six $3p$ electrons of Nb at around −32 eV in the DOS of both $NbAl_3$ and $NbGa_3$ and the 10 $3d$ electrons of Ga atom at around −16 eV in the DOS of $NbGa_3$. The wider valence band width of the DOS in $NbGa_3$ is mainly due to the s electrons of the Ga atoms. The low excitation bands (the band right above the Fermi level) of the two systems are very different, i.e., the very narrow band in $NbAl_3$ compared with the extended one in $NbGa_3$, while their first peaks are mainly from the p orbitals of Al in $NbAl_3$ but from the $3d$ orbitals in $NbGa_3$. Therefore the two systems can have very distinct electron transport properties.

From the calculated $N_d(E_F)$, we deduced $(1/T_1T)_d$ values which appear to be reasonable as compared to the experimental T_1 data. Results clearly indicate that $NbAl_3$ contains less Nb d-character Fermi-level DOS than $NbGa_3$. In general, the lower Fermi-level DOS is often related to the higher phase stability. This can be understood as follows: If the Fermi-level DOS is small, it means that more electrons participate in bonding and get localized. As a result, the stability of the material will be larger. With this accordance, the present study confirms that $NbAl_3$ is more stable than $NbGa_3$ with respect to the $D0_{22}$ structure, which is due to the stronger p-d hybridization in the former compound.

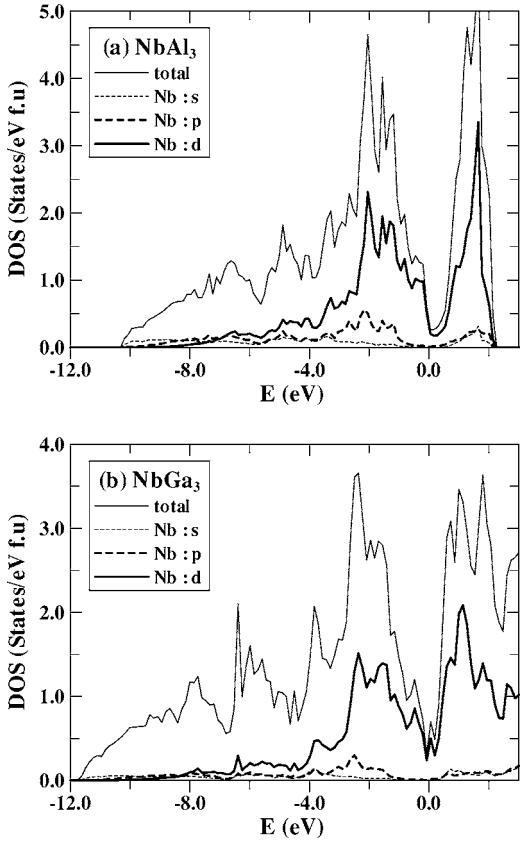

FIG. 4. Total density of states (the thin solid lines) for $NbAl_3$ (a) and $NbGa_3$ (b) and the corresponding orbital projected partial density of states for Nb atoms in the systems. The zero of the energy denotes the Fermi level of the system.

III. CONCLUSIONS

We have a concise picture of the NMR features for $NbAl_3$ and $NbGa_3$, giving experimental viewpoint for their local electronic properties. A strong similarity was found for the NMR characteristics of both materials, pointing to a uniformity in their electronic structures. Results of quadrupole interaction and anisotropic Knight shift provide a comparison of p-d hybridization for both materials. The spin-lattice relaxation rate together with the calculated $N_d(E_F)$ show some evidence that $N_d(E_F)$ correlates with the stability for the $D0_{22}$ structure.

ACKNOWLEDGMENTS

One of the authors (C.S.L.) was supported by the National Science Council of Taiwan under Grant No. NSC-95-2112-M-006-021-MY3. The computer resources were partially provided by the National Center for High Performance Computing in HsinChu, Taiwan.

*Electronic address: cslue@mail.ncku.edu.tw

[1] J. H. Schneibel, P. F. Becher, and J. A. Horton, J. Mater. Res. **3**, 1272 (1988).
[2] W. Lin, J. H. Xu, and A. J. Freeman, Phys. Rev. B **45**, 10863 (1992).
[3] M. Asta, D. de Fontaine, M. van Schilfgaarde, M. Sluiter, and M. Methfessel, Phys. Rev. B **46**, 5055 (1992).
[4] E. Cabet, A. Pasturel, F. Ducastelle, and A. Loiseau, Phys. Rev. Lett. **76**, 3140 (1996).
[5] S. Liu, R. Hu, and C. Wang, J. Appl. Phys. **79**, 214 (1996).
[6] C. Colinet, A. Pasturel, D. Nguyen Manh, D. G. Pettifor, and P. Miodownik, Phys. Rev. B **56**, 552 (1997).
[7] C. S. Lue, S. Chepin, J. Chepin, and J. H. Ross, Jr., Phys. Rev. B **57**, 7010 (1998).
[8] T. J. Bastow, C. T. Forwood, M. A. Gibson, and M. E. Smith, Phys. Rev. B **58**, 2988 (1998).
[9] M. Krajči and J. Hafner, J. Phys.: Condens. Matter **14**, 1865 (2002).
[10] C. L. Condron, G. J. Miller, J. D. Strand, S. L. Bud'ko, and P. C. Canfield, Inorg. Chem. **42**, 8371 (2003).
[11] M. Jahnatek, M. Krajči, and J. Hafner, Phys. Rev. B **71**, 024101 (2005).
[12] A. E. Carlsson and P. J. Meschter, J. Mater. Res. **4**, 1060 (1989).
[13] J. H. Xu and A. J. Freeman, Phys. Rev. B **40**, 11927 (1989).
[14] T. Hong, T. J. Watson-Yang, A. J. Freeman, T. Oguchi, and J. H. Xu, Phys. Rev. B **41**, 12462 (1990).
[15] M. Weinert and R. E. Watson, Phys. Rev. B **58**, 9732 (1998).
[16] W. B. Pearson, *A Handbook of Lattice Spacing and Structures of Metals and Alloys* (Pergamon, New York, 1958); *Smithells Metals Reference Book*, 6th ed., edited by E. A. Brandes (Butterworths, London, 1983).
[17] C. S. Lue, B. X. Xie, S. N. Horng, J. H. Su, and Y. J. Lin, Phys. Rev. B **71**, 195104 (2005).
[18] C. S. Lue, T. H. Su, B. X. Xie, S. K. Chen, J. L. MacManus-Driscoll, Y. K. Kuo, and H. D. Yang, Phys. Rev. B **73**, 214505 (2006).
[19] C. S. Lue, B. X. Xie, and C. P. Fang, Phys. Rev. B **74**, 014515 (2006).
[20] M. H. Cohen and F. Reif, *Solid State Physics* (Academic, New York, 1957), Vol. 5, p. 311.
[21] W. H. Jones, Jr., T. P. Graham, and R. G. Barnes, Phys. Rev. **132**, 1898 (1963).
[22] Y. Yafet and V. Jaccarino, Phys. Rev. **133**, A1630 (1964).
[23] W. Low, J. Appl. Phys. **39**, 1246 (1968).
[24] *Metallic Shifts in NMR*, edited by G. C. Carter, L. H. Bennett, and D. J. Kahan (Pergamon, Oxford, 1977).
[25] Shinji Wada, Ryozo Aoki, and Osamu Fujita, J. Phys. F: Met. Phys. **14**, 1515 (1984).
[26] J. Korringa, Physica (Amsterdam) **16**, 601 (1950).
[27] B. Nowak and O. J. Zogal, Solid State Nucl. Magn. Reson. **1**, 251 (1992).
[28] C. S. Lue and J. H. Ross, Jr., Phys. Rev. B **60**, 8533 (1999).
[29] P. Hohenberg and W. Kohn, Phys. Rev. **136**, B864 (1964).
[30] J. P. Perdew in *Electronic Structure of Solids '91*, edited by P. Ziesche and H. Eschrig (Akademie-Verlag, Berlin, 1991); J. P. Perdew, J. A. Chevary, S. H. Vosko, K. A. Jackson, M. R. Pederson, D. J. Singh, and C. Fiolhais, Phys. Rev. B **46**, 6671 (1992).
[31] W. Kohn and L. J. Sham, Phys. Rev. **140**, A1133 (1965).
[32] G. Kresse and J. Hafner, Phys. Rev. B **47**, 558 (1993); **49**, 14251 (1994); G. Kresse and J. Furthmüller, *ibid.* **54**, 11169 (1996); Comput. Mater. Sci. **6**, 15 (1996).
[33] P. E. Blöchl, Phys. Rev. B **50**, 17953 (1994).
[34] G. Kresse and D. Joubert, Phys. Rev. B **59**, 1758 (1999).
[35] H. J. Monkhorst and J. D. Pack, Phys. Rev. B **13**, 5188 (1976).